Theoretical and Applied Climatology (2021) 146:243–256
https://doi.org/10.1007/s00704-021-03728-4

ORIGINAL PAPER

Multistage spatiotemporal variability of temperature extremes over South China from 1961 to 2018

Leidi Wang[1] · Fei Hu[1] · Jing Hu[1] · Chen Chen[2] · Xian Liu[3] · Dingling Zhang[4] · Tingting Chen[1] · Yuchen Miao[1] · Lei Zhang[1]

Received: 15 March 2021 / Accepted: 11 July 2021 / Published online: 3 August 2021

Abstract

The variability of air temperature extremes exerts a great influence on agricultural production and the global hydrologic cycle. It has been the focus of attention for the past several decades. Using observed surface air temperature from 192 meteorological stations in South China maintained by the China Meteorological Administration, this study computed and analyzed 10 extreme temperature indices and the mean temperature at multiple spatiotemporal scales for the period from 1961 to 2018. These indices were analyzed with particular reference to the growing season of rice. Results showed that the variation trends of all annual indices exhibited different north–south patterns across decades, and the most recent 20-year period experienced greater warming than previous periods. The regional averaged rates of the annual mean maximum temperature, the annual mean minimum temperature, summer days, and tropical nights were 0.163 °C decade^{-1}, 0.197 °C decade^{-1}, 1.2 days decade^{-1}, and 5.4 days decade^{-1}, respectively. Except for the month of April, the southern region mostly experienced stronger warming than the northern region, especially in summer and autumn. Nighttime warming was usually greater than daytime warming, especially in June and October. Most temperature indices showed very weak correlations with large-scale atmospheric oscillations.

1 Introduction

Climate extremes have been extensively studied and changes in temperature extremes have been identified in many places (Brown et al. 2008; Fischer and Knutti 2015; Gao and Franzke, 2017; Wu et al. 2019; Abera et al. 2020). Hydrologists and meteorologists have documented how the changes of extreme hot or cold temperature events can increase agricultural and food crises (Piao et al. 2010; Sun and Huang 2011; Lobell et al. 2013; Chen et al. 2019; Karimzadeh Soureshjani et al. 2019; Eck et al. 2020). Analyzing changes in temperature extremes will greatly contribute to our understanding of the impacts of extreme temperatures on agricultural adaptation strategies, human society, and economy.

Because of differences in climatic background, driving forces, and regional characteristics, however, the variability of climatic extremes in different regions tends to be different (Li et al. 2010; Sun et al. 2014; Gao and Franzke 2017; Shi et al. 2018; Zhao et al. 2019; Niu et al. 2020). Meanwhile, local changes in temperature extremes affect agricultural production, crop layout, and cropping system, and ultimately drive mitigation policy (Sun and Huang, 2011; Zhang et al. 2016; Eck et al. 2020). Therefore, there is a great demand to detect the variations of temperature extremes at regional and local scales.

This study focused on the spatiotemporal variations of temperature extremes in South China. South China is one of the major agricultural production centers for double cropping rice, sweet corn, and spring and autumn peanuts, playing an important role in China's food security. Located in the subtropical and tropical latitudes, South China is characterized by high annual temperatures. Although the mean warming rate

Leidi Wang and Fei Hu equally contributed to this work

✉ Lei Zhang
zhanglei@scau.edu.cn

[1] College of Agriculture, South China Agricultural University, Guangzhou 510642, China

[2] Laboratory of Typhoon Forecast Technique, Shanghai Typhoon Institute, China Meteorological Administration, Shanghai 200030, China

[3] School of Earth Systems and Sustainability, Southern Illinois University Carbondale, Carbondale, IL 62901, USA

[4] College of Science, Northwest A&F University, Yangling 712100, China

in South China is less than that in other parts of China (Li et al. 2010; Shi et al. 2014), even slight warming can lead to agricultural disaster and falling crop yields (Peng et al. 2004; Moriondo et al. 2011; Lobell et al. 2013; Rosenzweig et al. 2014). Therefore, it is important and necessary to identify the spatial and temporal variations of temperature extremes in South China.

Many regions in South China, with the coastal area, in particular, showed significant positive trends for monthly mean temperatures and monthly maximum mean temperatures from 1961 to 2007 (Fischer et al. 2010). The warming was reflected mainly by the remarkable increase in the minimum temperature in the past decades (Zhang et al. 2011; 2013). South China has been experiencing increased hot extreme temperature events (Wei and Chen 2009; Zhang et al. 2014; Chen et al. 2016). South China has been experiencing decreased low-temperature extremes although it is still often hit by the extreme cold disaster (Sun and Huang 2011). The projection from the regional climate model showed an increase in extreme temperatures across the entire region in the following century (Wu and Huang, 2016). These studies, however, have focused mainly on interannual climatic variability, while crop sensitivity to temperature extremes is different for different stages of growth. Little data is available to demonstrate the temporal and spatial variations of temperature extremes at multiple timescales, particularly during the rice-growing season over the past 60 years in South China, which may affect our understanding of the impact of global warming on rice production.

Additionally, these changes in temperature extremes are related to regional climate warming and atmospheric circulation (Diffenbaugh et al. 2017; Gao and Franzke 2017). We applied many large-scale atmospheric circulation indices, such as the Arctic Oscillation, the El Niño–Southern Oscillation, and the North Atlantic Oscillation, to examine these relationships (Gao and Franzke 2017; Shi et al. 2018; Tong et al. 2019; Wu et al. 2019). Little research has been conducted, however, on the effects of multiple atmospheric circulation indices on the changes in extreme temperature events in South China. Therefore, a systematic study of temperature extremes in the growing season in South China is needed. This study focused on the long-term period and multistage spatiotemporal variability of both warm and cold temperature extremes in South China during the rice-growing season. The results provided not only a better understanding of the variations of temperature extremes in South China but also a scientific basis for disaster mitigation and food security.

2 Materials and methods

2.1 Study area and meteorological data

South China, located between 18° N–26° N and 104° E–117° E, consists of Guangdong Province, Guangxi Province, and Hainan Province. It is one of the major crop-producing regions in China, especially rice. In this study, South China only refers to the three Provinces' land parts. This study selected 192 meteorological stations each with a 58-year good data record (from 1961 to 2018). There are 85 stations in Guangdong, 88 stations in Guangxi, and 19 stations in Hainan distributed across the study area (Fig. 1). The daily data obtained from the China Meteorological Administration included daily mean temperature, daily maximum temperature, and daily minimum temperature (http://data.cma.cn/).

In addition, we used climate indices of several large-scale circulation patterns to assess their potential impacts on temperature extremes, based on large-scale circulation patterns impacting the climate in China (Gao and Franzke 2017; Wu et al. 2019; Tong et al. 2019). The large-scale oceanic atmospheric circulation indices selected in this study include the Arctic Oscillation (AO), the El Niño–Southern Oscillation (ENSO), the North Atlantic Oscillation (NAO), the Pacific Decadal Oscillation (PDO), the Southern Oscillation (SO), and the East Asian summer monsoon (EASM). We obtained the first five indices from https://www.esrl.noaa.gov/psd/gcos_wgsp/Timeseries/ and downloaded EASM from http://ljp.gcess.cn/dct/page/1. The Niño3.4 (5° S–5° N, 170° W–120° W) SST was used as an index for ENSO.

2.2 Methods

The Expert Team on Climate Change Detection and Indices (ETCCDI) has been coordinating an international effort to develop and analyze a suite of 16 temperature indices

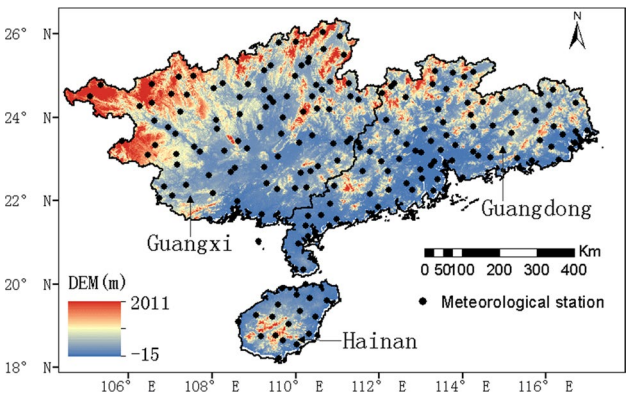

Fig. 1 Geographic location of the study area and meteorological stations in South China

(Easterling et al. 2003). Separate researchers have calculated the indices in exactly the same way, ensuring that the results are comparable across the world. Therefore, these indices have been widely used to examine changes in temperature extremes in the world. In this study, we selected the 10 most relevant indices for South China to reflect different aspects in temperature extremes (Table S1): growing season length (GSL), the numbers of summer days (SU_{25}), the numbers of tropical nights (TR_{25}), the mean maximum temperature (TX), the mean minimum temperature (TN), the diurnal temperature range (DTR), the monthly maximum of daily maximum temperature (TXx), the monthly maximum of daily minimum temperature (TNx), the monthly minimum of maximum temperature (TXn), and the monthly minimum of daily minimum temperature (TNn). Furthermore, we used three threshold values (10 °C, 15 °C, 20 °C) to determine the three kinds of GSL (GSL_{10}, GSL_{15}, and GSL_{20}, respectively), which would be more sensible for thermophilic crops like rice. We also analyzed the mean of the daily mean temperature (Tm) to supplement the temperature extremes. We divided these indices into two categories: the first category included the annual indices (Tm, TX, TN, DTR, GSL, SU_{25}, TR_{25}); the second included the monthly indices (TXx, TNx, Txn, and TNn). Meanwhile, it is easy to understand the three annual indices (Tm, TX, TN) also could be used as monthly indices.

This study focused mainly on the main growing season of rice from March 1 to October 31. As such, we based the decadal or annual mean of each temperature index, except for GSL, SU_{25}, and TR_{25}, at each station on the averaged value over the period from March 1 to October 31 rather than the whole calendar year. This study explored the variation characteristics of air temperature at four timescales: decadal, annual, monthly, and 10-day. According to Lobell et al. (2011), the distributions of temperature and precipitation trends after 1980 were different from those before 1980. Therefore, for the decadal timescale, this study used 1980 as the first demarcation point and used 2000 as the second demarcation point to keep the similar length of years for different periods. Our study divided the data of 58 years into three periods, namely, period 1 (P1, 1961–1979), period 2 (P2, 1980–1999), and period 3 (P3, 2000–2018). For the annual or monthly scale, our study averaged daily data over each year or month to obtain each observation for a certain year or month. For the 10-day scale, our study averaged daily data over three separate 10-day periods per month to obtain 24 observations per year.

The Theil–Sen (TS) median trend analysis method not only can help diminish the influence of missing time series observations but also can remove the outliers in time series (Sen 1968). So, this study applied the TS slope estimator to explore the variation rate within the time series. The calculation formula can be written as follows:

$$\beta = \text{Median}\left[\frac{x_i - x_j}{i - j}\right](\text{for } \; i = 1, 2, \ldots \ldots, n), \tag{1}$$

$$K = \beta \times 10, \tag{2}$$

where K indicates the variation rate within the time series; n is the number of data points; x_i and x_j are the sequential data at times j and i ($j > i$). A positive K-value indicates an increasing trend and a negative K-value indicates a decreasing trend;$K = 0$ means no change. The unit of the climatic trend rate K is °C decade^{-1} or days decade^{-1} in this study.

Because of its insensitivity to outliers and normally distributed time series data, the nonparametric Mann–Kendall (MK) test (Mann 1945) has been widely used in the long-term analysis of meteorological time series (Tong et al. 2019; Niu et al. 2020). This study used the MK trend test to determine whether the trends were significant. The value of the test statistic Z was used to compute the significance level. The significance levels of $p = 0.05$ and 0.01 were taken as the thresholds to identify a significant trend. The trend was significant at the 95% and 99% confidence levels if $|Z| > 1.96$ and $|Z| > 2.58$, respectively. In addition, we performed an independent samples t-test to test whether the regional temperature values were significantly different across decades. We also applied Pearson correlation analysis to measure the strength of the relationship between the regionally averaged temperature indices and atmospheric circulation patterns and tested their significance ($p < 0.05$).

This work not only identified the trends of regional temperature extremes based on the individual stations but also analyzed the regional trend patterns at decadal, annual, and monthly scales. We constructed spatial distributions using the inverse distance weighting interpolation method embedded in the ArcGIS software package.

3 Results

3.1 Temperature extremes analysis at decadal scale

To identify the overall background of surface air temperature in South China, Figure S1 shows the spatial distributions of the historical record of the annual indices for the entire study period. Although the values of GSL_{20} were smaller than GSL_{10} and GSL_{15}, the spatial distribution of GSL_{20} followed a similar pattern as that of GSL_{10} and GSL_{15}. So, the spatial distribution of GSL_{20} was not illustrated. Over the period from 1961 to 2018, Tm, TX, and TN in the southern region were generally higher than that in northern Guangdong and Guangxi Provinces. Hainan Province had the highest temperatures in general. This was directly attributable to the low latitude

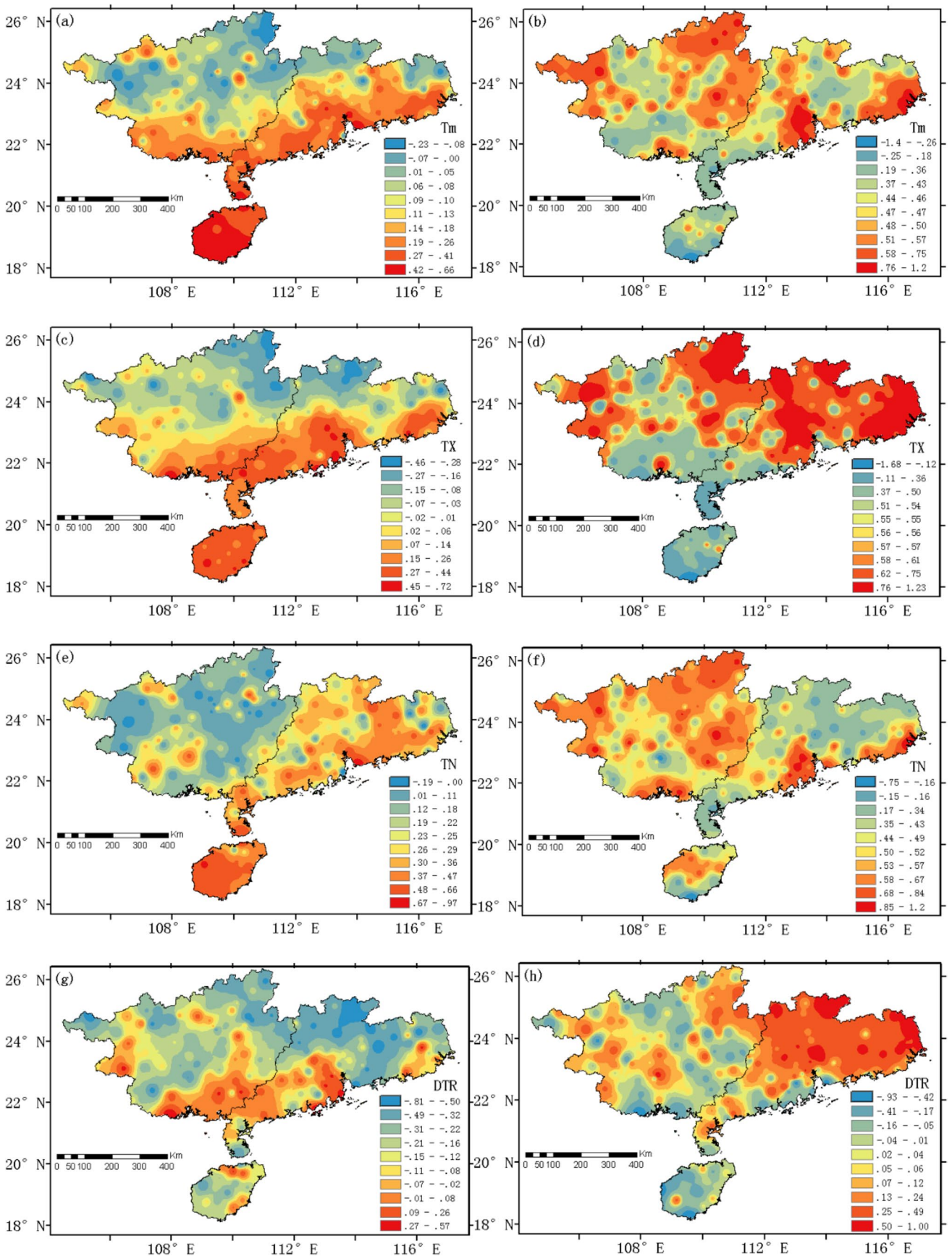
(a)
Tm
-.23 - -.08
-.07 - .00
.01 - .05
.06 - .08
.09 - .10
.11 - .13
.14 - .18
.19 - .26
.27 - .41
.42 - .66
(b)
Tm
-1.4 - -.26
-.25 - .18
.19 - .36
.37 - .43
.44 - .46
.47 - .47
.48 - .50
.51 - .57
.58 - .75
.76 - 1.2
(c)
TX
-.46 - -.28
-.27 - -.16
-.15 - -.08
-.07 - -.03
-.02 - .01
.02 - .06
.07 - .14
.15 - .26
.27 - .44
.45 - .72
(d)
TX
-1.68 - -.12
-.11 - .36
.37 - .50
.51 - .54
.55 - .55
.56 - .56
.57 - .57
.58 - .61
.62 - .75
.76 - 1.23
(e)
TN
-.19 - .00
.01 - .11
.12 - .18
.19 - .22
.23 - .25
.26 - .29
.30 - .36
.37 - .47
.48 - .66
.67 - .97
(f)
TN
-.75 - -.16
-.15 - .16
.17 - .34
.35 - .43
.44 - .49
.50 - .52
.53 - .57
.58 - .67
.68 - .84
.85 - 1.2
(g)
DTR
-.81 - -.50
-.49 - -.32
-.31 - -.22
-.21 - -.16
-.15 - -.12
-.11 - -.08
-.07 - -.02
-.01 - .08
.09 - .26
.27 - .57
(h)
DTR
-.93 - -.42
-.41 - -.17
-.16 - -.05
-.04 - .01
.02 - .04
.05 - .06
.07 - .12
.13 - .24
.25 - .49
.50 - 1.00
0 50 100 200 300 400 Km
26° N
24° N
22° N
20° N
18° N
108° E
112° E
116° E

◂**Fig. 2** Spatial distributions of air temperature difference across different periods (unit: °C): **a**, **c**, **e**, **g** P2 minus P1, **b**, **d**, **f**, **h** P3 minus P2. Note: period 1 (P1, 1961–1979), period 2 (P2, 1980–1999), and period 3 (P3, 2000–2018)

of the southern area. For DTR, the spatial mean was only 7.7 °C in South China. DTR was higher in northern South China and northwestern Hainan Province but lower in the southern Guangdong and Guangxi Provinces, which was also related to the higher Tm in the relatively low latitude areas.

As for GSL and SU_{25}, the southern region possessed a higher value than the northern region because of the relatively lower latitude. In Hainan Province and a partial region of southern Guangdong and Guangxi Provinces, the growing season was year-round, whereas the GSL was only about 200 days in the northern region. SU_{25} could be as high as 200 days in the southern region, whereas it was only about 140 days in the northern region. TR_{25} also had a much higher value in the southern region, except for some of the areas located in central Hainan Province. Regional averages for Tm, TX, and TN were 24.7 °C, 25.9 °C, and 17.6 °C, respectively. In the past 58 years, the regional mean GSL_{10}, GSL_{15}, GSL_{20}, SU_{25}, and TR_{25} were 340.5 days, 285.3 days, 212.3 days, 202.3 days, and 48.3 days, respectively. All of the indices in South China were much higher than those in most areas of China (Gao and Franzke 2017; Niu et al. 2020).

Figure 2 reveals the spatial distributions of temperature difference across different periods. The mean temperature and extreme temperatures (TX, TN, and DTR) differed among the different periods at a 99% confidence level. From P1 to P2, the mean temperature Tm increased significantly in southern South China, especially in Hainan Province (Fig. 2a, c, e, and g). However, Tm showed a decreasing trend in some of the northern regions. The spatial variations of TX and TN presented similar patterns as that of Tm. The amplification of Tm, TX, and TN was almost above 0.40 °C in all of Hainan Province. From P1 to P2, the spatial mean amplification of Tm, TX, and TN was 0.15 °C, 0.07 °C, and 0.25 °C, respectively. Conversely, there was a remarkable reduction in DTR for a large proportion of South China. The spatial mean difference of DTR between P1 and P2 was − 0.18 °C.

For the difference between P2 and P3, patterns of temperature extremes were inconsistent with those between P1 and P2 for a large portion of South China (Fig. 2b, d, f, h). In the most northern region, all four temperature indices increased from P2 to P3, whereas they decreased in many parts of southern South China, and the opposite trend was observed in P1 to P2. From P2 to P3, the spatial mean amplification of Tm, TX, TN, and DTR was 0.47 °C, 0.61 °C, 0.50 °C, and 0.11 °C, respectively.

GSL and SU_{25} had similar variation patterns as the previously discussed indices across the different periods. However, TR_{25} mostly increased in southern regions and decreased in a few northern regions across the different periods. Overall, the increased magnitudes of the temperature extremes from P2 to P3 were more remarkable than those from P1 to P2. On the regional average from P1 to P3, the increased magnitude of Tm, TX, and TN was 0.63 °C, 0.68 °C, and 0.75 °C, respectively. $GSL_{10,}$ GSL_{15}, and GSL_{20} increased about 5 days, 10 days, and 8 days, respectively. TR_{25} increased 22 days from P1 to P3, which was much higher than the increased magnitude of SU_{25} which increased only 5 days. The decreased magnitude of DTR was weak from P1 to P3 and originated from the fact that the increased magnitude of TN was a little higher than that of TX.

3.2 Temperature extremes analysis at annual scale

Figure 3 shows the trends and spatial distributions of the analyzed annual temperature indices. DTR is not shown in the figure because DTR was relatively stable over the course of the study period. GSL_{10} and GSL_{20} are not shown because they followed similar patterns to that of GSL_{15}. For Tm, TX, TN, and TR_{25}, 90.0% (173), 85.4% (164), 95.8% (184), and 88.0% (169) stations passed the significance test at the 95% level. For SU_{25}, about half of the stations, which are mostly located in central and east South China, passed the significance test at the 95% level. At a large portion of stations, patterns of Tm, TX, and TN were consistently warming with a high trend rate of more than 0.15 °C $decade^{-1}$ since 1961. Tm, TX, TN, and TR_{25} increased faster in the southern region than in other areas. GSL and SU_{25} had a more rapid warming in central and east South China with an increased rate of above 1.0 days $decade^{-1}$. TR_{25} had a larger increasing rate than SU_{25} in most southern regions with a rate as high as above 5.0 days $decade^{-1}$.

As for the regional mean, Tm, TX, and TN increased with a regionally averaged rate of 0.149 °C $decade^{-1}$, 0.163 °C $decade^{-1}$, and 0.197 °C $decade^{-1}$, respectively. For single station and regional mean, the trend rates of TX and TN had a slight difference. The regionally increasing rate of GSL_{10} and GSL_{15} was 1.3 days $decade^{-1}$, and 2.9 days $decade^{-1}$, respectively. The regionally averaged rate of SU_{25} was 1.2 days $decade^{-1}$, and the warming of TR_{25} was much larger with an average value of 5.4 days $decade^{-1}$.

3.3 Temperature extremes analysis at monthly scale

The previous analysis provides an overall picture of the temperature extreme variations throughout South China. This analysis, however, was not sufficient to represent the

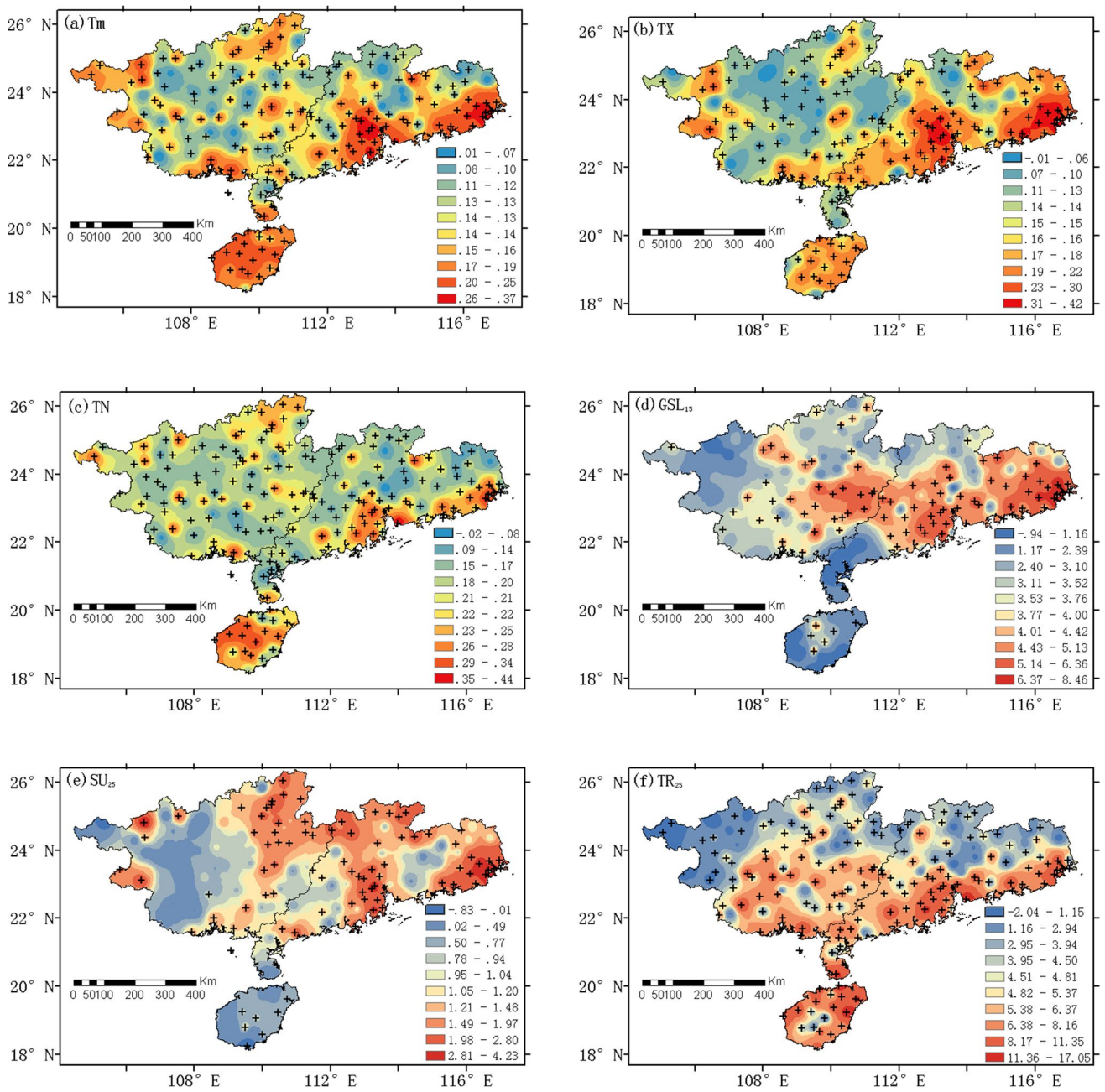

Fig. 3 Spatial distributions of the climatic trend rates of temperature indices at annual scale: **a** Tm, **b** TX, **c** TN (unit: °C decade^{-1}); **d** GSL_{15}, **e** SU_{25}, and **f** TR_{25} (unit: days decade^{-1}). Note: + trends at the 95% confidence level

variation details because the variation of the temperature may be uneven in each rice-growing period. This study further analyzed the annual and monthly indices at a monthly scale. Table 1 provides the mean climate inclination rate *K* for temperature indices at a monthly scale, and Table S2 shows the percentage of stations that passed the significance test. As demonstrated by Table 1 and Table S2, DTR insignificantly decreased at a very low rate in almost all of the months, and TXn insignificantly increased in most of the months. Most stations, however, recorded significant warming for Tm, TX, TN, TXx, TNx, and TNn in many months with most of those indices passing the 99% confidence level. The warming rates were more notable in April, June, August, September, and October. Therefore, we mainly focused on these six indices in those months that experienced significant changes.

Tm had a relatively weaker warming rate than TX and TN. TX had the greatest rate in June, and TN had the greatest increasing rate in October. Similarly, TXx significantly increased from April to September, with the highest rate

Table 1 Regional averaged climate inclination rate for temperature indices (°C decade^{-1}) at monthly scale in the main growth stage of rice

Month	Tm	TX	TN	DTR	TXx	TNx	TXn	TNn
Mar	0.151	0.101	0.210 [a]	−0.064	0.111	0.209 [a]	0.089	0.156
Apr	0.209[a]	0.231[a]	0.221[a]	−0.016	0.320 [a, b]	0.258 [a, b]	0.103	0.169
May	0.092	0.131[a]	0.105	−0.019	0.192 [a, b]	0.157[a, b]	0.110	0.176
Jun	0.189[a,b]	0.233[a,b]	0.227[a,b]	0.028	0.265 [a, b]	0.228[a, b]	0.156	0.365 [a, b]
Jul	0.048	0.052	0.111[a,b]	−0.041	0.173 [a, b]	0.154[a, b]	−0.026	0.176[a, b]
Aug	0.110[a,b]	0.149[a,b]	0.141[a,b]	0.008	0.219 [a, b]	0.181[a, b]	−0.072	0.120 [a, b]
Sep	0.157[a,b]	0.148[a]	0.193[a,b]	−0.034	0.225 [a, b]	0.201 [a, b]	0.021	0.227 [a]
Oct	0.222[a,b]	0.214[a,b]	0.256[a,b]	−0.054	0.116	0.193 [a, b]	0.257	0.502 [a, b]

[a]Statistically significant at the 95% confidence level

[b]Statistically significant at the 99% confidence level

of 0.320 °C decade^{-1} in April. TNx showed a significantly increasing rate with a magnitude between 0.154 and 0.258 °C decade^{-1} from April to October. Compared with TX and TXx, TN and TNx had greater increasing rates. TNn showed significant and remarkable warming between June and October with a highest average value of 0.502 °C decade^{-1} in October. The increasing rates of TNn were much higher than that of the other extreme indices in June, September, and October. This finding suggested stronger warming of air temperature in the nighttime.

To reveal the spatial distribution of extreme temperatures at the monthly scale from 1961 to 2018, Figs. 4, 5, 6 and 7 present the spatial variation trends for the four indices in the months with the significant trend rates: Fig. 4 for TX; Fig. 5 for TN; Fig. 6 for TXx; Fig. 7 for TNn (the figures for Tm and TNx were ignored). Generally, the rates of each temperature indices showed remarkable temporal and spatial nonuniformity. The trend rate of TX had a relatively similar spatial pattern as that of Tm. Therefore, the increase or decrease of TX partly contributed to the increase or decrease of Tm. In April, TX and Tm showed a remarkable increase in northern South China. The increasing rate of TX could reach about 0.52 °C decade^{-1} in the north, while the rate was really weak in the south.

In May, June, August, September, and October, however, the variation trends were mostly weaker in the north and stronger in the south. In those months, the significant increasing trends in TX were mainly observed in most areas of Hainan Province and the south of Guangdong Province, especially in the Pearl River delta with increasing rates frequently above 0.20 °C decade^{-1}. As for TNx, the great increasing rate for many months also appeared in the southern region. As for TN (Fig. 5), the trend rate of TN did not demonstrate the same regular north–south spatial distribution as that of Tm and TX. Except for July, TN increased in most regions with a high trend rate.

As illustrated in Fig. 6, TXx increased remarkably in the west area of Guangxi Province and some eastern areas of Guangdong Province in April and May with a maximum rate of above 0.60 °C decade^{-1}. In other months, TXx mostly showed a great increasing rate in eastern Guangdong Province. Meanwhile, Hainan Province experienced a significant increase in TXx in most months. The spatial patterns of TXx rates were relatively consistent with that of TX in many regions.

For TNn (Fig. 7), the warming rate also depicted the notable spatial inhomogeneity in each month from June to October with the trend rates significantly ranging from 0 to 1.03 °C decade^{-1}. In June, the strong warming mainly occurred in nearly all of Guangxi Province and western Guangdong Province, with the greatest rate reaching 0.67 °C decade^{-1}. In July, the greater warming rate occurring in Hainan Province and some areas of Guangxi Province. In August, September, and October, the greatest warming occurred in most areas of Guangdong Province and southern Guangxi Province. In October, the whole region observed the warming TNn, and the warming rate could even be above 1.0 °C decade^{-1} in southeastern Guangdong Province.

3.4 Temperature extremes analysis at 10-day scale

This study further explored the uneven variation of temperature extremes during the main rice growth period. Figure S2 shows the trend values of the 10-day average temperature within the annual cycle. The trends of the 10-day average temperatures were also uneven during each month. The warming of TX and TN exhibited a similar trend as Tm with the trend rate mostly increasing around 0.20 °C decade^{-1}. However, TX and TN mostly exhibited small differences in warming rate, and the variations of Tm, TX, and TN at 10-day scale were just partially significant. On the 110th day of the year, TX increased rapidly with an increasing rate of above 0.40 °C decade^{-1}, which was the largest trend rate over the course of the year. On the 160th day and 300th day of the year, the three temperature indices increased significantly with an increasing rate of around 0.30 °C decade^{-1}.

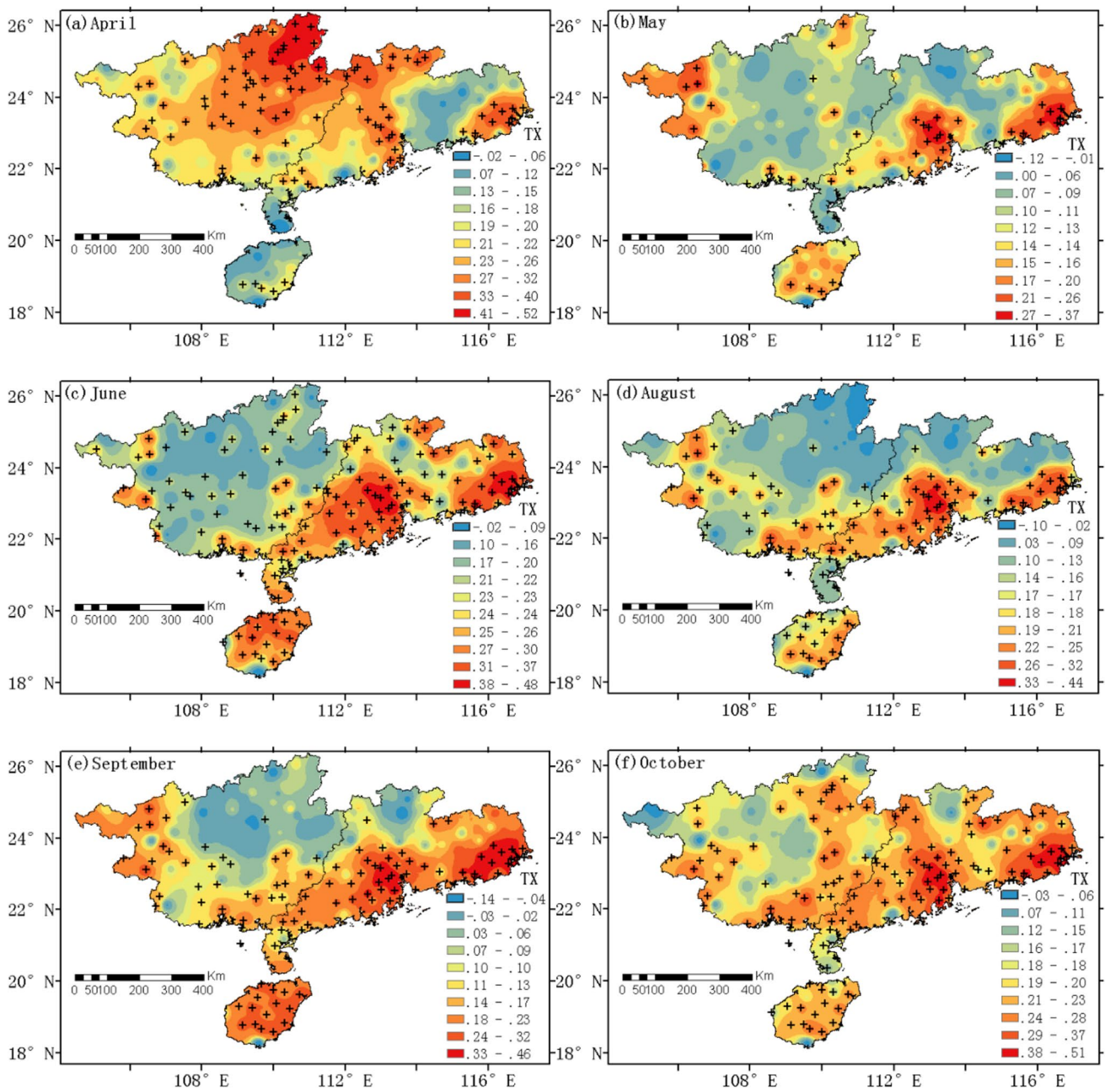

Fig. 4 **a–f** Spatial distributions of the climatic trend rates of TX in different months (unit: °C decade^{-1}). Note: + trends at the 95% confidence level

We also identified a significant increase for three indices with a warming rate of around 0.20 °C decade^{-1} on the 110th day of each year.

4 Discussion

Overall, most of South China experienced widespread significant warming during the past 58 years. Further having analyzed the accumulative temperature with Tm consecutively larger than 10 °C, we found that the accumulative temperature increased with a regionally averaged rate of 72.9 (°C day) decade^{-1}. From the decadal analysis, the previous study from Lobell et al. (2011) is supported by our finding related to the remarkable warming after the 1980s. In each period of the crop-growing season, the trend rates of each temperature index were profoundly spatially inhomogeneous in the past 58 years. The variation of TNn had the greatest spatial inhomogeneity. For a certain area, the variation rates varied from month to month and even from day to day, sometimes

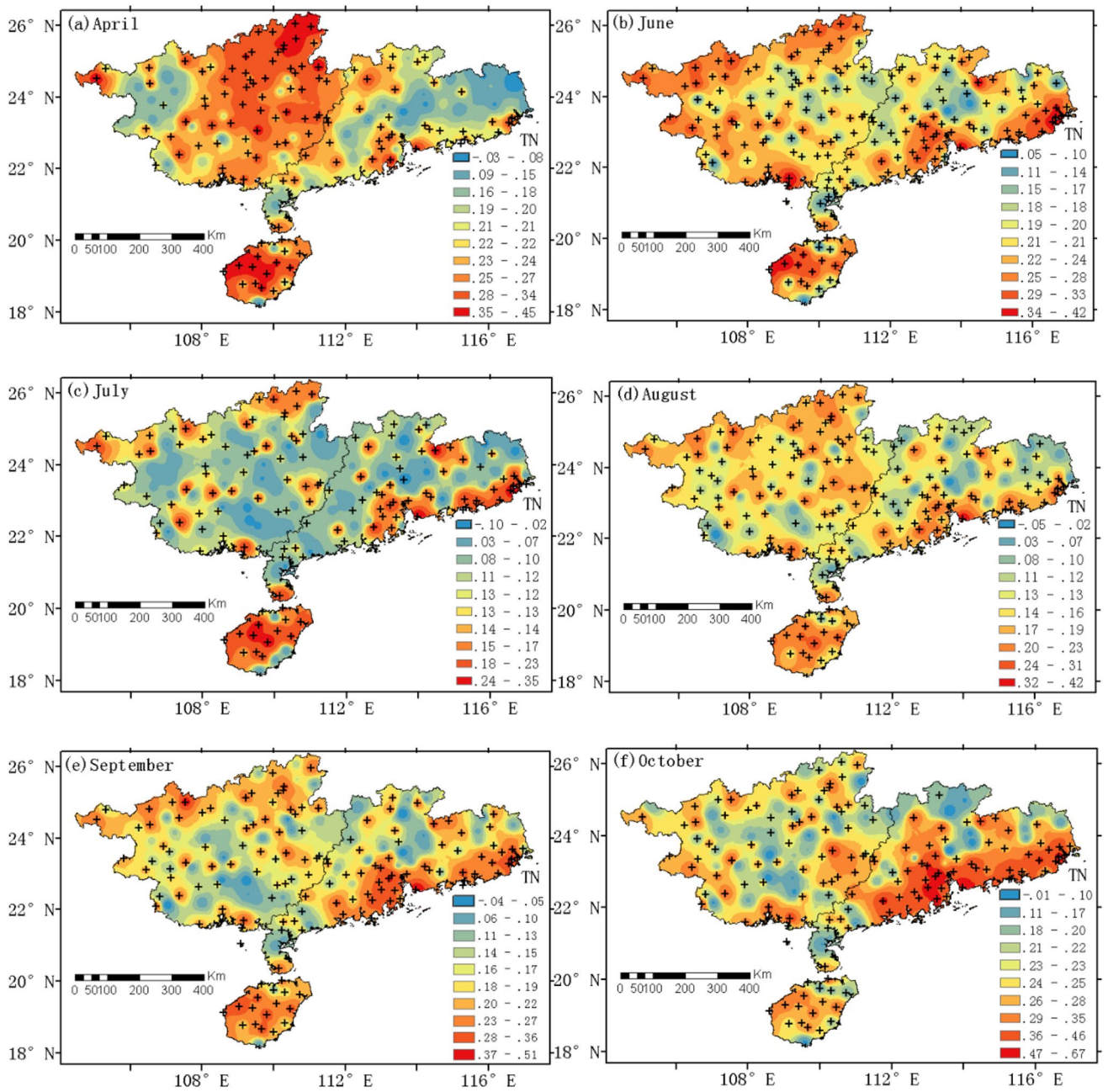

Fig. 5 **a**–**f** Spatial distributions of the climatic trend rates of TN in different months (unit: °C decade^{-1}). Note: + trends at the 95% confidence level

showing the opposite trend. Therefore, our work focusing on a multitemporal analysis was highly helpful for understanding the inhomogeneity of temperature variations.

Previous studies have shown increases in warm days and decreases in cold days over southern China (Wei and Chen 2009; Sun and Huang 2011; Zhang et al. 2014, 2016; Shi et al. 2018), which was partly consistent with the findings from our study to a certain degree. However, regional discrepancies of changes in temperature still exist. Our study identified significant warming in annual TX with a rate of 0.163 °C decade^{-1} from 1961 to 2018, which was a little weaker than that from 1961 to 2007 with a rate of 0.2 °C decade^{-1} (Fischer et al. 2010). The warming rate of TN was 1.2 times that of TX, and the warming rate of TR_{25} was 4.5 times that of SU_{25} from 1961 to 2018 in South China. On a global scale, the rate of increase of the land-surface daily minimum temperature over the past five decades was 1.4 times that of the daily maximum temperature (IPCC 2007). We can see that the differences in the warming rates between the low-temperature extremes and

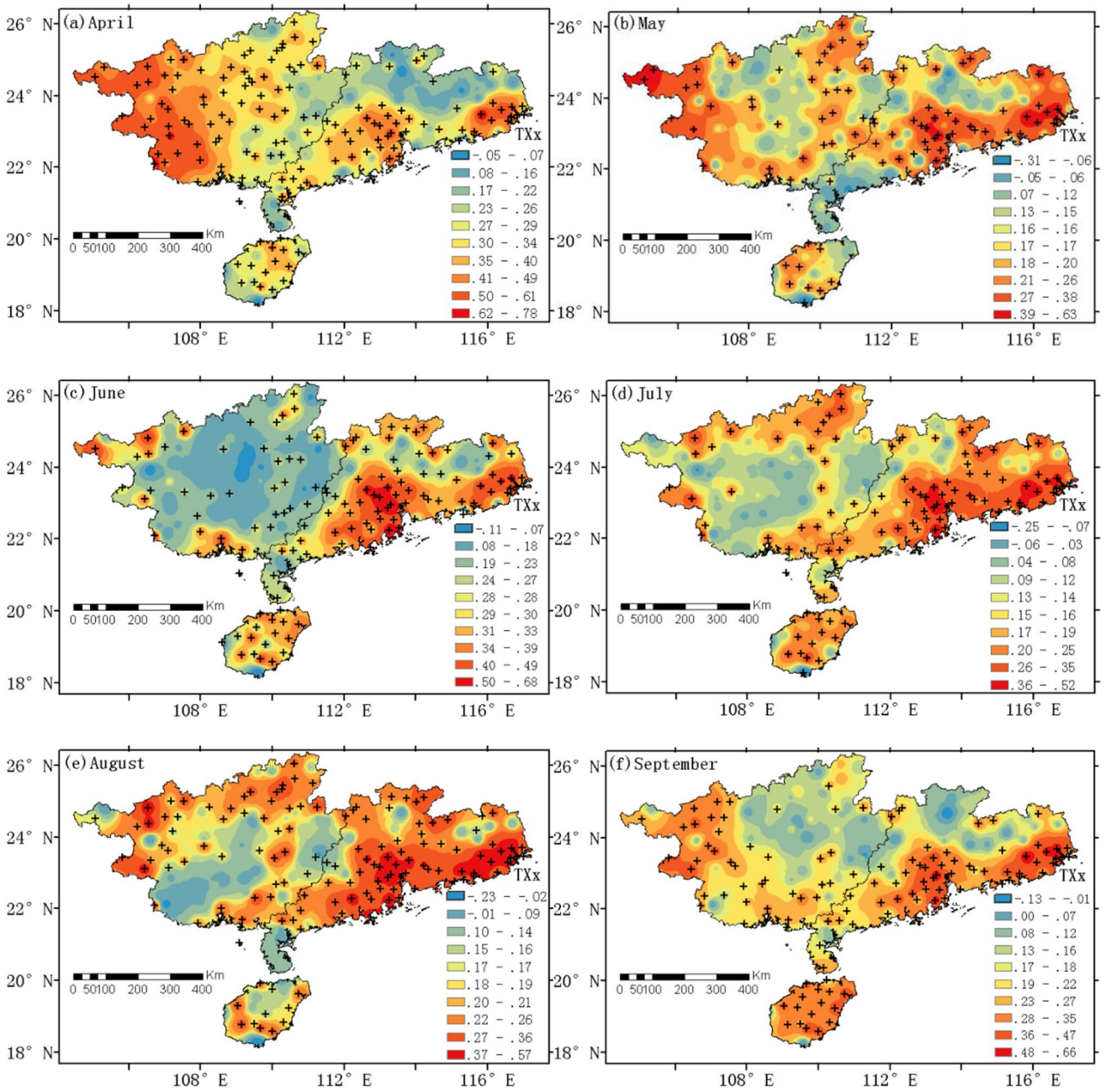

Fig. 6 **a**–**f** Spatial distributions of the climatic trend rates of TXx in different months (unit: °C decade^{-1}). Note: + trends at the 95% confidence level

the high-temperature extremes were very notable in South China at annual scale.

In addition, our study determined that some low-temperature indices had stronger warming rates than high-temperature indices, not only at annual scale but also at seasonal or monthly scale (i.e., in summer and autumn, the warming rate of TNn was larger than that of TXx). In other words, warming overnight was stronger than warming during the day in some months. For instance, the warming rate of TNn was 1.4 times that of TXx in June; the warming rate of TNn was 4.3 times that of TXx in October. Compared with the previous findings (Piao et al. 2010; Wu et al. 2019; Shi et al. 2018), the warming rates of low-temperature indices in South China were mostly higher than those in some other parts of China.

Conversely, the warming rate of TNn was smaller than that of TXx in spring, especially in April, which further displayed the temporal complexity of the variation rates for each index. Additionally, in October, TNn demonstrated a warming trend over all stations in South China, and the regional averaged TNn presented its highest rate of 0.502 °C

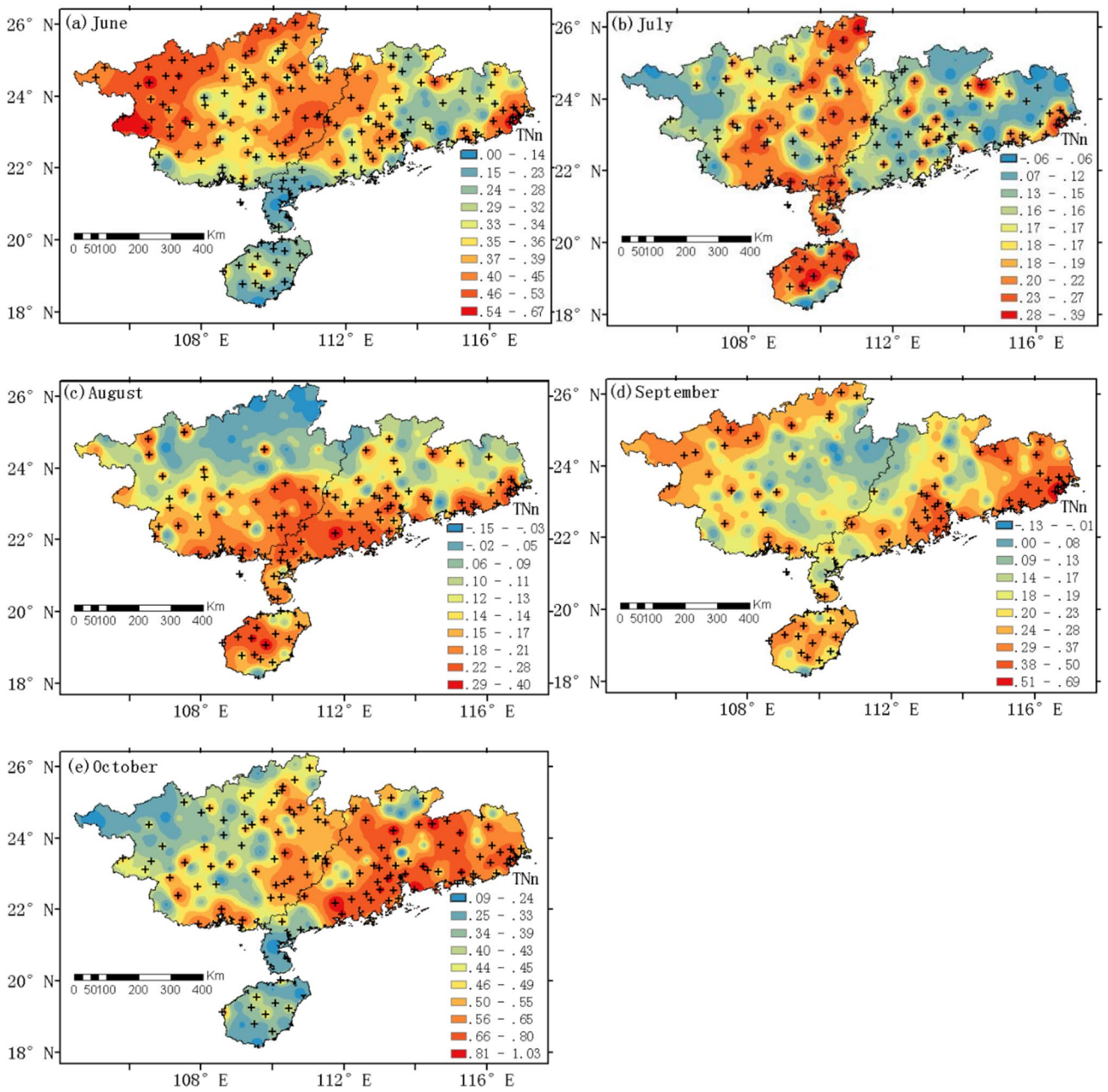

Fig. 7 **a**–**e** Spatial distributions of the climatic trend rates of TNn in different months (unit: °C decade^{-1}). Note: + trends at the 95% confidence level

decade^{-1}, which was much higher than that of the other extreme indices. Meanwhile, TX and TN mostly exhibited some differences in warming rate at 10-day scale. Overall, it is clear that the gaps of the asymmetric warming rates between high-temperature indices and low-temperature ones were different at different timescales.

This asymmetric warming can affect carbon assimilation and consumption by plants, which would lead to a divergent response of the vegetation growth and carbon sequestration to rising temperatures (Peng et al. 2013). Meanwhile, the greater warming in nighttime would not be good for the organic matter accumulation of crops in South China. Summer is the stage of spring rice reproductive growth, and autumn is the stage of autumn rice whole growth. This means that the autumn rice may suffer more from the extreme warming temperatures. The ideal temperature for rice, corn, and peanut is around 20–32 °C. The daytime temperatures frequently exceed the ideal growing conditions as a result of higher-than-normal maximum temperatures, and the higher-than-normal minimum temperatures during

critical crop development stages will lead to significant declines in crop productivity (Peng et al. 2004; Eck et al. 2020). Therefore, rice yields in South China will suffer considerable declines because of temperatures that frequently exceed ideal growing conditions, with the most significant losses occurring during the summer and autumn months.

As for the reasons for the variation in temperature extremes, many studies have demonstrated that atmospheric circulation change is an important mechanism affecting climate change in China (Gao and Franzke 2017; Wu et al. 2019; Tong et al. 2019; Niu et al. 2020). It is necessary to explore the influence that atmospheric circulation patterns have on temperature extremes in South China. We investigated potential connections between temperature extremes in South China and atmospheric circulation patterns by computing the Pearson correlation coefficient between extreme indices and the chosen atmospheric circulation indices from 1961 to 2018 (Table 2). There was a significantly and weakly positive correlation between Nino3.4 and the six temperature indices, Tm, GSL_{20}, SU_{25}, TX, TN, and TNx, all with coefficients as high as above 0.30. EASM had a weak negative influence on TR_{25}, TN, and TNx with coefficient values around 0.3. SO was negatively correlated with SU_{25} with a coefficient value of 0.27 at the confidence level of 95% but generally was insignificantly negatively correlated with other temperature extremes. AO, NAO, and PDO generally were insignificantly positively correlated with temperature extremes.

This result indicated that the trends in temperatures extremes were weakly related to the large-scale atmospheric circulations over South China. However, the large-scale atmospheric circulations mostly displayed significant correlations with the temperature extremes in some regions of China (Gao and Franzke 2017; Wu et al. 2019; Tong et al. 2019; Niu et al. 2020). It further indicates that the contribution of those atmospheric circulation patterns to extreme climate events differs from region to region, which enhanced the significance of our study in South China.

Furthermore, urban warming has contributed to approximately one-third of China's increased temperatures over the time period from 1961 to 2013 (Sun et al. 2016). The contribution of urbanization to warming trends in temperature cannot be ignored (IPCC 2007). According to Zhao et al. (2014), the area of farmland has decreased 3063.82 km^2 in Guangdong Province, 208.44 km^2 in Guangxi Province, and 165.63 km^2 in Hainan Province with 68.26%, 72.20%, and 43.76% of missing farmland being transformed into urban construction land for each province, respectively. This change has resulted in the replacement of green spaces with impervious surfaces.

Urbanization, with changes in regional land use and land cover, can affect a plant's ability to store carbon and mitigate climate change and can decrease evaporation and latent heat flux as well as partition more energy into sensible heat in the affected regions (Yu et al. 2019). Furthermore, urbanization accompanied by the urban heat island effect has a significant influence on local temperatures, with large cities displaying stronger positive effects on warm temperature indices (Chapman et al. 2017; Zhao et al. 2019). Compared with the northern regions, southern South China, with more big cities, was affected more by land use changes and frequent human activity following urbanization. The local climate was profoundly affected in southern South China, with some variations in extreme temperatures maybe being ascribed to rapid local urbanization and dense population.

Table 2 Pearson's correlation coefficients between the extreme temperature indices and the atmospheric circulation indices

Month	AO	Nino3.4	NAO	PDO	SO	EASM
Tm	0.099	0.353 [a]	0.037	0.070	−0.252	−0.249
GSL_{10}	0.226	0.035	0.112	0.023	−0.065	−0.109
GSL_{15}	0.198	−0.032	0.162	−0.265	0.091	0.036
GSL_{20}	−0.071	0.353 [a]	−0.008	−0.077	−0.240	−0.016
SU_{25}	−0.098	0.373 [a]	−0.085	−0.065	−0.268 [a]	−0.042
TR_{25}	0.117	0.157	−0.021	0.156	−0.076	−0.316 [a]
TX	0.023	0.325 [a]	−0.021	0.025	−0.211	−0.150
TN	0.163	0.307 [a]	0.050	0.078	−0.212	−0.283 [a]
DTR	−0.217	−0.009	−0.107	−0.089	0.028	0.106
TXx	0.215	0.132	0.029	0.078	−0.078	−0.253
TNx	0.076	0.303 [a]	−0.036	0.240	−0.210	−0.307 [a]
TXn	0.054	0.103	0. 039	0.135	−0.139	0.037
TNn	0.137	0.165	0.003	0.254	−0.144	0.036

[a]Significant at the 95% confidence level

5 Conclusions

This study investigated the temporal and spatial evolution of temperature extremes from 1961 to 2018 considering the main rice growth period at multiple temporal and spatial scales in South China. The extreme temperature indices showed remarkably different trends and spatial inhomogeneity across three periods (P1, 1961–1979; P2, 1980–1999; P3, 2000–2018). From P1 to P2, all annual indices of interest (Tm, TX, TN, DTR, GSL, SU_{25}, and TR_{25}) significantly increased in some southern regions, whereas they mostly revealed cooling trends in many northern regions. From P2 to P3, however, those annual indices mostly showed an opposite trend from P1 to P2 for the north and the south at a broad spatial scale. The amplitude of temperature increase in the recent 20-year period was higher than that in the previous decades.

From 1961 to 2018, by contrast with a weaker rate in the north-central region, annual extreme temperatures did increase strongly in a large portion of the southern region. The regional average rate of TX, TN, SU_{25}, and TR_{25} was 0.163 °C decade^{-1}, 0.197 °C decade^{-1}, 1.2 days decade^{-1}, and 5.4 days decade^{-1}, respectively. The warming rate of TR_{25} was much higher than that for the daytime index SU_{25}.

In April, June, August, September, and October, the significant warming of the extreme temperature indices TX, TN, TXx, and TNx was most notable, and the increase in the southern region was mostly larger than that in the northern region except for the month of April. TNn significantly increased in summer and autumn, and warming occurred over all stations in October. In summer and autumn, the increase in extreme low-temperature indices TN and TNn was larger than that in extreme high-temperature indices TX and TXx.

Large-scale atmospheric oscillations only slightly contributed to variations in extreme temperatures in South China, with only Nino3.4, EASM, and SO having a weak correlation with few extreme temperature indices. These results underscored the need for further research on the impact of anthropogenic factors on regional and local climate change.

In the near future, southern South China would be much warmer than the northern region. Rice yields in South China will suffer considerable declines with the most significant losses occurring in the southern region. It is needed to pay great attention to the influence of temperature extremes on rice during summer and autumn months. Our findings highlight the necessity of developing integrated adaption strategies to ensure food security.

Supplementary Information The online version contains supplementary material available at https://doi.org/10.1007/s00704-021-03728-4.

Acknowledgements We would like to thank the China Meteorological Administration (CMA) for providing the meteorological data.

Author contribution Leidi Wang and Fei Hu analyzed the data and wrote the paper. Jing Hu and Chen Chen assisted in data processing and analysis and interpreted the results. Xian Liu and Dingling Zhang assisted in drawing and writing the original draft. Tingting Chen and Yuchen Miao participated in data curation and validation. Lei Zhang designed the study and participated in writing-editing.

Funding This work was supported by the National Natural Science Foundation of China (grant number 42005142, 41605118) and the Key Science and Technology Planning Project of Guangdong Province (grant number 2019B020214003).

Data availability All the data are available in the public domain at the links provided in the texts.

Code availability The codes used for the processing of data can be provided on request to the corresponding author.

Declarations

Ethics approval The authors confirm that this article is original research and has not been published or presented previously in any journal or conference in any language.

Consent to participate Not applicable.

Consent for publication All the authors consented to publish the paper.

Conflict of interest The authors declare no competing interests.

References

Abera TA, Heiskanen J, Pellikka P, Maeda EE (2020) Impact of rainfall extremes on energy exchange and surface temperature anomalies across biomes in the Horn of Africa. Agric For Meteorol 280:107779

Brown SJ, Caesar J, Ferro CAT (2008) Global changes in extreme daily temperature since 1950. J Geophys Res 113:D05115

Chapman S, Watson JEM, Salazar A et al (2017) The impact of urbanization and climate change on urban temperatures: a systematic review. Landscape Ecol 32:1921–1935

Chen W, Zhu D, Huang C et al (2019) Negative extreme events in gross primary productivity and their drivers in China during the past three decades. Agric for Meteorol 275:47–58

Chen Y, Zhang L, Qian H (2016) Variation characteristics and spatial differences of extremely high temperature days over South China during the recent 53 Years. Trop Geogr 36(4):692–699

Diffenbaugh NS, Singh D, Mankin JS et al (2017) Quantifying the influence of global warming on unprecedented extreme climate events. Proc Natl Acad Sci 114(19):4881–4886

Easterling DR, Alexander LV, Mokssit A, Detemmerman V (2003) CCI/CLIVAR workshop to develop priority climate indices. Bull Am Meteor Soc 84(10):1403–1407

Eck MA, Murraya AR, Wardc AR et al (2020) Influence of growing season temperature and precipitation anomalies on crop yield in the southeastern United States. Agric For Meteorol 291:108053

Fischer T, Gemmer M, Liu L, Su B (2010) Trends in monthly temperature and precipitation extremes in the Zhujiang River Basin, South China (1961–2007). Adv Clim Chang Res 1(2):63–70

Fischer EM, Knutti R (2015) Anthropogenic contribution to global occurrence of heavy-precipitation and high-temperature extremes. Nat Clim Chang 5(6):560–564

Gao M, Franzke CL (2017) Quantile regression–based spatiotemporal analysis of extreme temperature change in China. J Clim 30(24):9897–9914

IPCC (2007) Climate change 2007: the physical science basis. Contribution of Working Group I to the Fourth Assessment Report of the Intergovernmental Panel on Climate Change. In: Solomon S, Qin D, Manning M, Chen Z, Marquis M, Averyt KB, Tignor M and Miller HL (Eds.). Cambridge University Press, Cambridge, United Kingdom and New York, NY, USA

KarimzadehSoureshjani H, GhorbaniDehkordi A, Bahador M (2019) Temperature effect on yield of winter and spring irrigated crops. Agric For Meteorol 279:107664

Li QX, Dong WJ, Li W et al (2010) Assessment of the uncertainties in temperature change in China during the last century. Chin Sci Bull 55(19):1974–1982

Lobell DB, Hammer GL, McLean G et al (2013) The critical role of extreme heat for maize production in the United States. Nat Clim Chang 3(5):497–501

Lobell DB, Schlenker W, Costa-Roberts J (2011) Climate trends and global crop production since 1980. Science 333(6042):616–620

Mann HB (1945) Nonparametric tests against trend. Econometrica J Econometric Soc 13:245–259

Moriondo M, Giannakopoulos C, Bindi M (2011) Climate change impact assessment: the role of climate extremes in crop yield simulation. Clim Change 104(3–4):679–701

Niu Z, Wang L, Fang L et al (2020) Analysis of spatiotemporal variability in temperature extremes in the Yellow and Yangtze River basins during 1961–2014 based on high-density gauge observations. Int J Climatol 40(1):1–21

Peng S, Huang J, Sheehy JE et al (2004) Rice yields decline with higher night temperature from global warming. Proc Natl Acad Sci 101(27):9971–9975

Peng S, Piao S, Ciais P et al (2013) Asymmetric effects of daytime and night-time warming on Northern Hemisphere vegetation. Nature 501:88–92

Piao S, Ciais P, Huang Y et al (2010) The impacts of climate change on water resources and agriculture in China. Nature 467(7311):43–51

Rosenzweig C, Elliott J, Deryng D et al (2014) Assessing agricultural risks of climate change in the 21st century in a global gridded crop model intercomparison. Proc Natl Acad Sci 111(9):3268–3273

Sen PK (1968) Estimates of the regression coefficient based on Kendall's tau. J Am Stat Assoc 63(324):1379–1389

Shi J, Cui L, Ma Y et al (2018) Trends in temperature extremes and their association with circulation patterns in China during 1961–2015. Atmos Res 212:259–272

Shi PJ, Sun S, Wang M et al (2014) Climate change regionalization in China (1961–2010). Sci China Earth Sci 57(11):2676–2689

Sun W, Huang Y (2011) Global warming over the period 1961–2008 did not increase high-temperature stress but did reduce low-temperature stress in irrigated rice across China. Agric for Meteorol 151(9):1193–1201

Sun Y, Zhang XB, Ren GY et al (2016) Contribution of urbanization to warming in China. Nat Clim Chang 6:706–709

Sun Y, Zhang XB, Zwiers FW et al (2014) Rapid increase in the risk of extreme summer heat in Eastern China. Nat Clim Chang 4(12):1082–1085

Tong S, Li X, Zhang J et al (2019) Spatial and temporal variability in extreme temperature and precipitation events in Inner Mongolia (China) during 1960–2017. Sci Total Environ 649:75–89

Wei K, Chen W (2009) Climatology and trend of high temperature extremes across China in summer. Atmos Oceanic Sci Lett 2(3):153–158

Wu CH, Huang GR (2016) Projection of climate extremes in the Zhujiang River basin using a regional climate. Int J Climatol 36:1184–1196

Wu X, Hao Z, Hao F, Zhang X (2019) Variations of compound precipitation and temperature extremes in China during 1961–2014. Sci Total Environ 663:731–737

Yu ZW, Yao YW, Yang GY et al (2019) Spatiotemporal patterns and characteristics of remotely sensed region heat islands during the rapid urbanization (1995–2015) of southern China. Sci Total Environ 674:242–254

Zhang Q, Li JF, Chen YD, Chen X (2011) Observed changes of temperature extremes during 1960–2005 in China: natural or human-induced variations? Theoret Appl Climatol 106(3–4):417–431

Zhang Q, Li JF, Singh VP, Xiao M (2013) Spatio-temporal relations between temperature and precipitation regimes: implications for temperature-induced changes in the hydrological cycle. Glob Planet Chang 111:57–76

Zhang S, Tao FL, Zhang Z (2016) Changes in extreme temperatures and their impacts on rice yields in southern China from 1981 to 2009. Field Crop Res 189:43–50

Zhang W, Jin FF, Turner A (2014) Increasing autumn drought over southern China associated with ENSO regime shift. Geophys Res Lett 41(11):4020–4026

Zhao N, Jiao Y, Ma T et al (2019) Estimating the effect of urbanization on extreme climate events in the Beijing-Tianjin-Hebei region, China. Sci Total Environ 688:1005–1015

Zhao XL, Zhang ZX, Wang X et al (2014) Analysis of Chinese cultivated land's spatial temporal changes and causes in recent 30 years. Trans Chin Soc Agric Eng 30(3):1–11 (In Chinese)